Anti-cancer effect of hUC-MSC-derived exosome-mediated delivery of PMO-miR-146b-5p in colorectal cancer

siming Yu
Department of Pharmacy, Peking University Shenzhen Hospital
ran Liao
Biotherapy Center, Harbin Medical University Cancer Hospital
lu Bai
Biotherapy Center, Harbin Medical University Cancer Hospital
madi Guo
Biotherapy Center, Harbin Medical University Cancer Hospital
yu Zhang
Biotherapy Center, Harbin Medical University Cancer Hospital
yumin Zhang
Biotherapy Center, Harbin Medical University Cancer Hospital
qi Yang
Biotherapy Center, Harbin Medical University Cancer Hospital
yushuai Song
Department of Gastrointestinal Medical Oncology, Harbin Medical University Cancer Hospital
zhiwei Li
Department of Gastrointestinal Medical Oncology, Harbin Medical University Cancer Hospital
qingwei Meng
Department of Medical Oncology, Harbin Medical University Cancer Hospital
shubin Wang
Department of Oncology, Shenzhen Key Laboratory of Gastrointestinal Cancer Translational Research, Cancer Institute, Peking University Shenzhen Hospital,Shenzhen-Peking University-Hong Kong University
xiaoyi Huang (xyhuang@hrbmu.edu.cn)
Biotherapy Center, Harbin Medical University Cancer Hospital

Research Article

Keywords: Exosomes, hUC-MSCs, drug delivery, miR-146b-5p, CRC, EMT

Posted Date: June 2nd, 2022

DOI: https://doi.org/10.21203/rs.3.rs-1704679/v1

Abstract

Background

Antisense oligonucleotide (ASO) is a novel therapeutic platform for targeted cancer therapy. Colorectal cancer (CRC) is the third leading cause of cancer mortality and the prognosis of CRC is poor when hepatic metastasis occurs. We have demonstrated that miR-146b-5p plays an important role in CRC progression. Knocking down miR-146b-5p by an ASO is expected to slow down the progression. However, a safe and effective strategy for delivery of an ASO to its targeted RNA remains as a major hurdle in translational advances.

Results

Human umbilical cord mesenchymal cell (hUC-MSC)-derived exosomes were used as vehicles to deliver an anti-miR-146b-5p ASO (PMO-146b) to CRC cells. PMO-146b was assembled onto the surface of exosomes(e) through a covalently conjugated anchor peptide CP05(P) that recognized an exosomal surface marker, CD63, forming a complex named ePPMO-146b. The conjugate (ePPMO-146b) was taken up by SW620 cells and effectively inhibited cellular proliferation and epithelial-to-mesenchymal transition. It also exerted antitumor efficacy in a xenograft mouse model of colon cancer by systematic administration, where PPMO-146b was enriched in tumor tissue. Of particular importance was selective distribution of ePPMO-146b in liver compared to native exosomes through *in vivo* imaging, indicating its therapeutic potential to inhibit hepatic metastasis of CRC.

Conclusion

Our study highlights the potential of hUC-MSC-derived exosomes anchored with PPMO-146b as a novel safe and effective approach for ASO delivery.

Introduction

Over the past decades, the focus of the pharmaceutical and biotechnology industries on anticancer agents has transitioned from traditional cytotoxic drugs to precisely targeted therapies. Advances in nanotechnology have shed light on engineered agents, which offer the potential for crossing biological barriers and performing transmembrane deliveries. Exosomes are a class of natural biological nanoparticles, are the smallest extracellular vesicles[1], with sizes falling between 50 and 150 nm, and are secreted from different types of cells through the endolysosomal pathway[2, 3]. Nanosized vesicles have the capacity to carry a wide variety of cargoes such as nanodrugs, functional proteins and antisense oligonucleotides (ASOs), like miRNAs, anti-miRNAs and small interfering RNAs (siRNAs)[4]. Due to their low immunogenicity, low toxicity, good biocompatibility, ability to be biodistributed to specific cells and tissue, and ability to transfer their contents into recipient cells via endocytosis, exosomes are leveraged on these characteristics to be ideal delivery strategies of therapeutic molecules as cell-free therapeutics[5, 6]

Mesenchymal stem cells (MSCs) are easily accessible, and can be derived from different sources such as bone marrow, placenta, adipose tissue and umbilical cord, therefore, MSCs are believed to be the most prolific producers of exosomes[7, 8]. MSC-derived exosomes as vehicles that can carry therapeutic molecules such as miRNA and siRNA, have been widely explored. Lou et al. observed that miR-199a-modified exosomes from adipose tissue-derived MSCs effectively sensitized hepatocellular carcinoma (HCC) to chemotherapies by targeting the mTOR pathway[9]. Another group reported that siGRP78-modified bone marrow MSCs (BM-MSCs)-derived exosomes could reverse the drug resistance of HCC cells to Sorafenib[10]. The first engineered MSC-derived exosomal therapy that carried KRAS G12D siRNA has entered clinical trails to treat pancreatic cancer (NCT03608631)[11]. In addition, this engineered exosomal platform that carried STAT3 siRNA or an ASO showed potential to ameliorate liver fibrosis[12]. Despite of the therapeutic value of modified MSC-derived exosomes, their translation to clinical practice is still hindered by the search for a feasible approach that enhances the *in vivo* delivery efficacy and supports convenient and sustainable production.

Colorectal cancer (CRC) is the third leading cause of cancer mortality worldwide[13, 14]. Even after chemotherapy, the prognosis of mCRC is still poor, and the 5-year survival rate is less than 20% because of the toxicity and poor tolerance of patients to chemotherapy [14]. Hundreds of studies have indicated that microRNAs (miRNAs) are key regulators in CRC cell invasion and metastasis by facilitating epithelial-to-mesenchymal transition (EMT)[15–17]. EMT is essential for promoting tumor invasion and metastasis in CRC[18]. We previously reported that miR-146b-5p (miR-146b) significantly promoted EMT phenotypes through Smad4 in CRC cells[19]. An in vivo study has demonstrated that miR-146b may play a tumor-promoting role in establishment of colorectal tumor [20, 21]. To therapeutically modulate miR-146b expression, we employed a synthetic anti-miR-146b ASO (PMO-146b) that are complementary to the mature miR-146b. Synthetic anti-miRNA oligonucleotides (PMOs) are believed as a new class of therapeutic agents specifically inhibiting individual miRNAs. However, the major challenge in applying PMO for clinical use is its insufficient cellular uptake[22, 23].

Herein, we evaluated whether the hUC-MSC-derived exosome carrying PMO-146b could inhibit CRC progression. PMO-146b is a phosphorodiamidate morpholino oligomer (PMO)[1, 24]. Quality-controllable exosomes that were sustainably generated by hUC-MSCs were verified by performing nano flow cytometry (NanoFCM). We then loaded the PMO-146b conjugated to the CP05 peptide (CRHSQMTVTSRL) on the surface of exosome. CP05 peptide has been shown to bind to tetraspinin CD63 enriched on the exosomal membrane[25–27]. Systemic administration of exosomes loaded the CP05 and PMO-146b conjugate (ePPMO-146b) was evaluated for safety and efficacy both *in vitro* and *in vivo* and demonstrated a therapeutic effect in a CRC mouse model. The present study indicates that MSC-derived exosome-anchored with an ASO may serve as a promising strategy for anti-mCRC therapy.

Methods And Materials

MSCs and tumor cell lines

Human umbilical cord MSCs (hUC-MSCs) were obtained from the Biotherapy Center of Harbin Medical University Cancer Hospital and prepared following a well-established protocol[28]. The human umbilical cords were donated by women who had underwent eutocia. Informed consents was obtained from the subjects' families and the study was approved by the Harbin Medical University Cancer Hospital Ethics Review Board. Purity was confirmed by flow cytometry (CD73+, CD90+, CD105+, and CD146+, CD31-, CD34-, CD45-, HLA-DR-). These MSCs can differentiate into osteoblasts, chondroblasts and adipocytes *in vitro*. MesenCult™ MSC Basal Medium (Stem Cell) was used to culture MSCs without serum in a GMP-grade condition. The 4^{th} passage was used for the following experiments. The differentiation of MSCs to adipocytes, osteocytes and chondrocytes was tested by using StemPro® and an adipogenesis kit (cat no.A10070-01, Gibco), osteogenesis kit (cat no.A10072-01, Gibco) and chondrogenesis differentiation kit (cat no.A10071-01, Gibco). Afterward, staining with Oil Red Oranse, Alizarin Red S, and Alcian Blue was also performed to detect adipocytes, osteocytes and chondrocytes, respectively.

The normal colonic mucosa cell line NCM460 was purchased from the Shanghai Cell Bank. The human HCT116 colorectal carcinoma (ATCC CCL-247™), SW480 adenocarcinoma carcinoma (ATCC CCL-228™), Caco2 adenocarcinoma carc carcinoma (ATCC HTB-37™), Lovo colorectal adenocarcinoma (ATCC CCL-229™), HT29 adenocarcinoma adenocarcinoma (ATCC HTB-38™) and SW620 colorectal adenocarcinoma [American Type Culture Collection (ATCC)® CCL-227™] cell lines were purchased from the ATCC. With the exception of Caco2, the other cell lines were grown in DMEM (Gibco) supplemented with 10% fetal bovine serum (FBS) and 1% antibiotic–antimycotic solution in a 5% CO_2 incubator. Caco2 cells were cultured in DMEM supplemented with 20% FBS.

Isolation and purification of research-grade exosomes

hUC-MSC-derived exosomes were purified by ultracentrifugation. Supernatants were collected from MSCs cultured as monolayers in serum-free medium and were subsequently subjected to centrifugation at 3,000 × g for 30 min. The supernatants were then filtered using 0.2-μm filters, and the pellet was recovered and subsequently ultracentrifuged (Beckman, USA) at 100,000 × g using a SW32 Ti rotor for 3 h. The supernatants were aspirated and the resulting pellet was suspended

again in PBS and again centrifuged at 100,000 × g for 1 h. The supernatants were aspirated and the pellet was recovered in 2 mL PBS and stored ar -80℃ until use.

Transmission electron microscopy (TEM)

The exosome suspension was diluted with PBS at a 1:1 ratio, and 10 μL of this solution was dropped onto formvar-carbon-coated grids and blotted with filter papers after sedation for 1 min. Then, 10 μL of 3% phosphotungstic acid was dropped onto the exosome area for 1 min. After the excess staining buffer was removed with filter papers, the grid was left to air-dry for 5 min. Exosome morphologies were visualized using a high-resolution transmission electron microscope (Hitachi HT7700, Japan) at 80 kV.

Nano flow cytometry (NanoFCM) for exosome size and concentration analysis

Flow NanoAnalyzer model type N30 (NanoFCM Inc., China) was used to determine the exosome size distribution and granular concentration according to the manufacturer's instructions. Briefly, the isolated exosomes were diluted with PBS at a 1:100 ratio. The Silica Nanospheres Cocktail (S16M-Exo, NanoFCM Inc., China) was employed to construct a calibration curve regarding particle size and side scattering intensity. Using this calibration curve, the side scattering intensity of every exosome was converted into the corresponding vesicle size.

Flow cytometry analysis of exosome-bound beads

Exosomes from MSCs were isolated as described above and resuspended in 200 μL PBS. Aldehyde/sulfate latex beads (10 μL, A37304, Life Technologies, USA) were added to the solution and mixed using a benchtop rotator for 15 min at room temperature. PBS (600 μL) was then added to the solution and mixed overnight at 4°C. The mixture was then spun down at 8,000 × g for 1 min. The precipitate was then resuspended in 100 μL of 10% BSA in PBS and mixed for 45 min at room temperature. The mixture was spun down at 8,000 × g for 1 min, and the supernatant was aspirated. Exosome-bound beads (the pellet) were then resuspended in 20 μL PBS and immunolabeled for CD63, CD73, CD90 or an isotype control. The beads were incubated with 1 μL anti-CD63 antibody (Catalog #12-0639-42, eBioscience, USA) or 1 μL anti-CD73 (Material Number 550257, BD Biosciences, USA) or 1 μL anti-CD90 antibody (Material Number 555596, BD Biosciences, USA) or 1 μL Mouse IgG1, κ isotype control antibody (Material Number 555749, BD Biosciences, USA) in a final volume of 20 μL and mixed at room temperature for 30 min in the dark. The mixture was then centrifuged at 8,000 × g for 1 min, the supernatant was aspirated, and the pellet was resuspended in 200 μL PBS with 2% BSA. The expression of exosomal markers (CD63) and mesenchymal markers (CD73 and CD90) was analyzed using flow cytometry (BD FACSAria II analyzer, USA). Data were analyzed using FlowJo software (TreeStar Inc.). The flow cytometry experiment was repeated two times independently using the same exosome preparation.

Synthesis of antisense oligomers

The morpholino oligos (also known as PMOs) were synthesized by Gene Tools LLC. (USA), including negative controls (NC) and anti-miR-146b-5p ASO (PMO-146b), all of which were modified on the 3' ends-biotin and 5' ends-primary amine. The purity of PMO was determined to be 95% using reverse-phase HPLC and MALDI TOF mass spectrometry. PMO sequences are listed in Supporting Information Table S1. The peptide CRHSQMTVTSRL (CP05) was conjugated with PMO-146b (PPMO-146b) as previously described[25, 29].

Flow cytometry and fluorescence microscopy

To measure the binding affinity of candidate peptides to exosomes (e), 1.32×10^{10} e were preincubated with biotin-labeled CP05-anti-miR-146b-5p ASO (PPMO-146b) or biotin-labeled anti-miR-146b-5p ASO (PMO-146b; as a control) overnight at 4°C (PPMO-146b or PMO-146b solution (10 μg/μL) resolved in PBS at 1 mM), followed by washing with PBS for five times in 1.5-mL ultracentrifuge tubes and filtration with Amicon Ultra-0.5 Centrifuge Filter (Millipore) to remove unbound peptides (14,000 g, 10 min). Subsequently, the exosome-PMO complexes, ePPMO-146b and ePMO-146b were incubated with 4-μm

aldehyde/sulfate latex beads for 15 min at room temperature under rotation and washed with PBS for three times (8,000 g, 1 min each time). The segregated complexes were then incubated with 3% BSA-DPBS for 30 min on a rotator. After washing with PBS for 3 times (8,000 g, 1 min), streptevidin-PE (1:500, diluted in 3% BSA blocking buffer, Catalog Number 12-4317, eBioscience) was added to the complexes and incubated for 30 min at room temperature in the dark. After washing 3 times with PBS, the recovered beads were observed with a conventional fluorescence microscopy (Zeiss, Germany) or subjected to flow cytometry (FACSCalibur, BD). Uncoated beads were used as negative controls for gating. We used the separation index (SI) metric that was defined by Theodoraki et. al, which takes into account both the difference in mean fluorescent intensity (MFI) between PPMO-146b and PMO-146b SI = $\frac{\left(MFI_{PPMO-146b} - MFI_{PMO}-146\text{b}\right)}{\sqrt{\frac{SD_{PPMO-146b}{}^{2} + SD_{PMO-146b}{}^{2}}{2}}}$ capture beads, and the average of their distributions[30].

Uptake of PKH67-labeled ePPMO-146b by SW620 cells

To determine whether SW620 CRC cells could take up targeted exosomes from hUC-MSCs, the PKH67 Green Fluorescent Cell Linker Kit (Thermofisher) was used to label exosomes, according to the manufacturer's protocol. Briefly, MSC-derived exosomes, ePMO-146b-biotin and ePPMO-146b-biotin were diluted and resuspended in sterile PBS to a final concentration of 5×10^{7} particles. Diluent C (500 μL; 2×PKH67 solution) was added to 2-μL PKH67 dye (PKH67GL, Sigma), and 500 μL exosomes were mixed with 500-μL PKH67 solution to allow internalization. Subsequently, incubate the exosomes/dye mixture for 1-5 min with periodic mixing, and then the staining was stopped by adding an equal volume of serum or 1% BSA-PBS. Then, the unbound PKH67 was removed by using Amicon Ultra-0.5 Centrifuge Filter (Millipore) at 14,000 × g for 10 min.

SW620 cells were seeded in 12-well plates at a density of 1×10^{5} cells/well and were incubated in a complete medium for 12 h. Subsequently, the plates were rinsed twice with PBS and fixed with 4% paraformaldehyde solution at 4℃. The plates were then rinsed again three times using PBS. After rewashing, 10 μM unlabeled avidin (S888, Invitrogen, USA) was added to link biotinylated PMO on the membrane surface for 30 min at 4℃.

Next, the cells were permeabilized with 0.1% Triton X-100 for 5 min. PBS with 3% BSA was used to incubate with the cells for 2 h to block nonspecific binding. Then Streptavidin R PE (SNN1007, Invitrogen, USA) was utilized for the detection of PMO-labeled biotinylated anti-miR-146b-5p ASO in presence or absence of CP05 peptides at room temperature for 1 h. Cells incubated with native exosomes and PBS with the same volume as the suspension of PMO-146b-loaded exosomes served as controls.. Finally, the cells were washed three times with precooled PBS and were mounted with DAPI-containing mounting media (H-1800, Vector Labs). Images were captured under a fluorescence microscope (Zeiss, Germany).

Quantitative real-time PCR

Total RNA was extracted from seven cell lines with TRIzol reagent (Invitrogen). The cDNAs were produced from the RNA samples with PrimeScript™ 1st Strand cDNA Synthesis Kit (No. 6110A, TaKaRa, Japan). Human U6 snRNA was used as an endogenous control for data normalization. Real-time PCR was performed on the LightCycler®96 system (Roche, USA) using TB Green™ Premix Ex Taq™ (No. RR820L, Takara, Japan). Relative miRNA expression was determined using the Ct method. All experiments were performed at least three times. Oligonucleotides were synthesized by Integrated DNA Technologies (Sangon Biotech, China) and the primer sequences were designed as previously described[19]. The primer sequences are listed in Table S1.

Cell viability analysis with a by CCK8 assay

SW620, Caco2 and Lovo cells were seeded in 96-well plates at a density of $5\text{-}8\times10^{4}$ cells/well. Once the cells reached an approximately about 80% confluency, they were starved overnight and cocultured with different concentrations of exosomes (2×10^{9}, 2×10^{10} and 2×10^{11} particles/mL) or an equal volume of PBS as a control. In another experiment, the cells were

exposed to exosomes, ePNC, ePPMO-146b or PBS. Cell growth was analyzed 48 h after the exosome treatment. CCK8 solution of 10 μL (Beyotime, China) was added to each well and the solutions were incubated at 37 °C for 4 h, then the optical density was detected at a wavelength of 450 nm by a microplate reader (Thermofisher, USA). The data shown are representative of at least three independent experiments.

Wound-healing assay

SW620 and Caco2 cells were seeded onto a six-well plate at a density of 5×10^5 cells/mL until they reached full confluency. The cells were cultured for 24 h in the presence of exosomes, ePNC or ePPMO-146b. Then each well was scratched by using a 200-μL pipette tube to create 2 linear regions that were devoid of cells, and medium without FBS was added. PBS was used as an additional negative control. Photographs were captured by a digital single lens reflex camera (Canon) at 0 and 24 h, respectively. The migration area of the cells was measured by ImageJ software.

Transwell migration assay

SW620 and Caco2 cells ($4\text{-}5\times10^4$ cells/well) were seeded on upper chambers (6.5 mm Transwell® with 8.0-μm pore polycarbonate membrane insert; Corning) in serum-free medium with 0.1% BSA. A total of 600 μL medium containing 10% FBS was added to the lower chambers. After incubation for 24 h, nonmigrating and noninvading cells were gently removed with a cotton swab. The cells were then fixed with methanol for 30 min and stained with 0.1% crystal violet for another 20 min. The area of dyed pores was then calculated under a microscope at a magnification of ×200. Three views were selected randomly for photography and analysis. Each measurement was repeated three times.

Western blot analysis

Total proteins from cells or exosomes were extracted at 4°C by using RIPA Lysis Buffer (Beyotime, China) with a protease inhibitor (Roche, USA), and were then vortexed every 5-10 min for 30 min. Subsequently, the lysates were spun down at 14,000 × g for 20 min to remove any debris and the supernatant was collected. Exosomes (20 μg) and protein samples (70 μg per lane) were loaded onto 10% SDS-PAGE gels and transferred onto PVDF membranes (Millipore, USA) for 90 min. For immunodetection, the membranes were incubated with the following primary antibodies at 4°C overnight: CD63 (ab134045), CD81 (ab109201), TSG101 (ab125011), E-cadherin (ab76055), vimentin (ab92547), and N-cadherin (ab76011). All primary antibodies were purchased from Abcam (Cambridge, UK).The next morning, the membranes were washed with TBS-T three times for 10 min each time. After incubation with secondary antibody at room temperature for 1 h, the membranes were washed with TBS-T and then incubated with luminol substrate solution (Transgene, China) for 1 min. Images were collected with a chemiluminescence imaging system (Proteinsimple). All experiments were performed at least three times.

In vivo experiments

Our protocol for animal use in this project was approved by the Animal Experimentation and Ethics Committee of Harbin Medical University Cancer Hospital and Peking University Shenzhen Hospital, and all animal experiments were carried out according to the Guide for the Care and Use of Laboratory Animals, and in strict accordance with the People's Republic of China Legislation Regarding the Use and Care of Laboratory Animals.

Antitumor efficacy of ePPMO-146b in tumor-xenografted nude mice

Adult female athymic BALB/c nude mice (15-20 g) that were 8 weeks old, were purchased from Beijing Vital River Laboratory Animal Technology Co., Ltd. [Certificate no. 110011211106810132 SCXK (Jing) 2021-0006]. The animals were housed in a controlled environment at 23±2°C under a 12-h dark/light cycle with free access to irradiated food and sterile water. To ensure the number of tumor-bearing mice, 10 female BALB/c nude mice were subcutaneously injected with Lovo cells in 200-μL of PBS (2×10^6 cells). One week later, the tumor-bearing mice were approximately 90 mm^3 in size. The tumor-bearing mice were randomly divided into ePNC group and ePPMO-146b group (n=5) on the basis of their tumor volume. EPNC solution and ePPMO-146b solution (5.0×10^{10} particles/kg in 10 μL) were injected into the tumor-bearing mice via a peritoneal injection. The

mice were treated twice a week for 24 days and tumor size was measured once or twice a week for 24 days with a vernier caliper. Tumor volumes were calculated according to the following formula: Volume (mm^3) = length × $(width)^2/2$. The mice were killed at 25 days post-injection of ePNC and ePPMO-146b. The inhibitory rate of tumor volume was calculated as IR (%) = $(V_t–V_0)/V_0 \times 100\%$, where V_0 is the tumor volume of the epNC group mice and V_t is the tumor volume of the ePPMO-146b group. The inhibitory rate of tumor weight was calculated as IR (%) = $(W_t–W_0)/W_t \times 100\%$, where W_t and W_0 represent the tumor weights of the ePNC and ePPMO-146b-treated groups, respectively.

Biodistribution of systemical ePPMO-146b

DiR-labeled exosomes were prepared according to the literature [31]. Purified exosomes (5.0×10^9 particles/mL) were incubated with 1 μM fluorescent lipophilic tracer DiR (D12731, Invitrogen, USA) for 5 min at 37℃ prior to 4℃ for another 15 min. Unbound dye was removed by centrifugation at 100,000 g overnight by means of an SW41 Ti rotor (Backman), and then the pellet was washed twice with precooled PBS. The obtained DiR-Exos were resuspended in precooled PBS, and the particle concentration was measured by nanoFCM. DiR-Exos were diluted in PBS to achieve a particle concentration of 8.0×10^9/mL.

Female healthy male C57BL/6N mice (Animal Center of the 2nd Affiliated Hospital of Harbin Medical University) or C57BL/6 nude mice aged 8 weeks were used. Freshly purified DiR-labeled exosomes and naked exosomes were injected intraperitoneally (i.p.) in the C57BL/6N mice. The biodistribution of DiR-labelled exosomes was examined using the same dosage mentioned above, and the particle count was measured with nanoFCM and the samples were diluted to 200 μL. To analyze DiR exosome distribution, IVIS Spectrum (Perkin Elmer) was performed. Live mice (isoflurane sedated) were imaged after 3 h posttreatment. For *ex vivo* imaging, the mice were sacrificed after 6 h postinjection and the liver, heart, lung, kidney, spleen, intestine and reproductive organs were collected. The live mice or the harvested organs were imaged for 1-2 seconds (at an excitation wavelength: 640 nm, and an emission wavelength of 710 nm).

DiR-ePPMO-146b was intraperitoneally injected in the tumor-bearing C57BL/6 nude mice. At 6 h postinjection (5.0×10^{10} particles/kg), organs were harvested and prepared as described above.

Statistical analysis

Statistical comparisons among multiple groups were determined by one-way analysis of variance (ANOVA) with Dunnett's post-hoc test. A probability value of 0.05 was considered to be significant. The results are expressed as the mean ± SEM.

Results

Characterization of MSCs and MSC-derived exosomes

We first characterized the identities of hUC-MSCs. The human umbilical cords were cultured for more than 4 weeks and spindle-shaped fibroblasts were observed (Fig. S1A). In addition, the multilineage differentiation potential of MSCs was demonstrated by Oil Red O staining, Alizarin Red staining and Alcian Blue staining (Fig S1B). MSCs are known to express cell surface markers like cluster of differentiation CD29, CD44, CD73, CD90 and CD105, but to lack CD14, CD34, CD45 or human leucocyte antigen-DR (HLA-DR)[32]. The flow cytometry analysis revealed that our isolated hUC-MSCs were positive for CD73, CD90, CD105 and the stemness marker CD146, but negative for CD34, CD45 or HLA-DR indicating that the cultured cells exhibited MSC-like features (Fig S1C).

To prepare exosomes, 500 mL MSC conditioned medium was centrifuged, and 10^{10}-$10^{11}$of exosomes were purified. Isolated MSC exosomes were validated in terms of their morphology, size and specific markers using TEM, nanoFCM analysis and Western blotting. Through TEM, it was observed that the exosomes exhibited typical disc shapes (Fig. 1A). The exosomes diameter ranged from 50 to 150 nm based on NanoFCM analysis and the mean diameter was ~69.04 nm (Fig. 1B). For exosomal surface markers, MSCs, supernatant and exosomes were loaded onto SDS-PAGE gels. The presence of CD63, CD81 and tumor susceptibility gene 101 protein (TSG101), which are commonly enriched in exosomes, was confirmed in MSCs-

derived exosomes using Western blotting (Fig 1C). In addition, flow cytometry revealed that the proportions of CD63+, CD73+ and CD90+ particles were 86.9%, 71.9% and 88.2%, respectively, indicating that the exosomes had an MSC origin. (Fig. 1D).

Optimization of PMO-146b-modified exosomes

In our previous study, we have determined that miR-146b promoted EMT in CRC indicating its potential as a therapeutic target[19]. To deliver anti-miR-146b into cells effectively and safely, exosomes were turned into viable nanocarriers for transferring the PPMO-146b conjugate. As illustrated by our Graphical Abstract, the PMO or CP05 peptide-PMO (PPMO) conjugates anchored onto the exosomes surface. To determine the optimal ratio of exosomes and PPMO (PPMO-146b conjugates), conventional flow cytometry was used. We successfully stained nanosized exosomal drug delivery vehicles that were loaded with PMO(PMO-146b cargo) or PPMO, and measured the MFI and SI of the oligonucleotides carried by exosomes. The optimal ratio of the exosomes/PMO was determined by titrations as illustrated in Figure 2. Increasing moles of biotinylated PMO or PPMO were co-incubated with 1.32×10^{10} beads/exosomes complexed with streptavidin-PE. The fluorescence intensity is a result of (1) the positive level of PMO-biotin and (2) its density on exosomes. This result is best described by the ratio of MFI of stained PPMO to MFI of stained PMO, the significance of which is determined by the SI. MFI of exosomes treated with 10 nmol PPMO was 2.3-fold higher than that of PMO. Meanwhile, 10 nmol PMO/PPMO showed the highest SI value 0.9, reflecting a significant separation between PPMO and PMO peaks (Fig 2A). The optimal ratio was also demonstrated using fluorescence microscopy (Fig 2B). These results indicated the potential of CP05 peptide-conjugated exosomes to be an appropriate delivery vehicles for various types of therapeutic oligonucleotide agents including but not limited to PMO-146b.

ePPMO-146b inhibited the proliferation of CRC cells

To investigate whether host cells could take up exosomes and whether CP05 affects the cellular internalization of exosomes, SW620 cells were incubated with PKH67-labeled (green fluorescence) native exosomes or biotinylated PMO-146b-loaded PKH67-labeled exosomes. After 12 h of cytoplasmic green staining, it was observed that a great number of exosomes were taken up by the SW620 cells (Fig 3A, upper line). Compared with native exosomes, ePMO-146b and ePPMO-146b achieved significantly higher cellular uptakes of PMO in SW620 cells, suggesting that MSCs-derived exosomes were able to efficiently deliver PMO to recipient cells (Fig 3A, middle line and bottom line). In the SW620 cells treated with ePPMO-146b (Fig 3A, bottom line), significantly stronger streptavidin-PE signals (red fluorescence) were dispersed with a punctate pattern in the cytoplasm compared with that of the ePMO-146b group (Fig 3A, middle line), indicating that using CP05 to anchor cargo to exosomes could facilitate the cellular internalization of oligonucleotides.

To determine whether exosomes that are loaded with CP05-modified PMO-based anti-miR-146b oligonucleotides to exert their inhibitory function in CRC, appropriate cell lines were screened, and the cellular viabilities of these lines were assessed. Aberrant upregulation of miR-146b was observed in CRC tissue[20]. Our qRT–PCR also verified that a higher expression level of miR-146b occurred in the six CRC cell lines than in the colonic epithelial NCM460 cells (Fig 3B). The results showed that the two highest groups were SW620 and Caco2 cells, with fold changes of 3.36±1.11 and 5.13±0.7, respectively. As a result, SW620 and Caco2 cells were selected to investigate the therapeutic effect of ePPMO-146b. Native exosomes that are derived from MSCs may promote the proliferation of parental cells[33, 34]. Therefore, a dose-titration study of MSC-derived exosomes was performed using a CCK8 assay. Among the six CRC lines, Lovo cells had the strongest protumorigenic properties in xenograft nude mice in our laboratory, thus the viability of LoVo cells was also examined. We then optimized the dose of native exosomes *in vitro* under various conditions and 5-FU (3 mM) was used as a positive control. MSC-derived exosomes at a concentration of ~10^{11} particles/mL accelerated cellular proliferation at 48 h, while up to ~10^{10} particles/mL MSC-derived exosomes did not have this effect(Fig. 3C). According to calculations, the optimal exosome concentration for the *in vitro* study was 2.6×10^{10} partiles/mL.

We then investigated the role of ePPMO-146b in the proliferation of SW620, Caco2, and Lovo cells (Fig 3D). Cellular viability was significantly decreased following a treatment with ePPMO-146b for 48 h (the viability rate: 58.86% for SW620, 80.14% for

Caco2 and 66.71% for Lovo). On the other hand, ePNC had no significant effect on cellular proliferation, which was probably due to the minimal cytotoxicity of this exosomal delivery system.

ePPMO-146b inhibits CRC cell metastasis by hampering EMT

A decrease in the migratory and invasive abilities of the CRC cells treated with AMO (anti-miRNA oligonucleotides)-miR-146b was observed in previous study[19-21], but whether ePPMO-146b exerted equal or even stronger effects remained unclear. Hence, wound healing and transwell assays were performed. ePPMO-146b-treated CRC cells resulted in a decrease in the migration (the inhibitory rate: 90.06% for SW620 cells and 85.27% for Caco2 cells; Fig 4A, B and E). Additionally, through the transwell assay, it was demonstrated that the cell number in the bottom chamber was decreased significantly by ePPMO-146b, indicating that ePPMO-146b markedly suppressed migration *in vitro* (Fig 4C, D, and F).

We previously reported that miR-146b can stimulate EMT promoting CRC cell invasion and metastasis[19, 20]. Therefore, whether ePPMO-146b could influence the EMT process of SW620 and Caco2 cells is a relevant question in the current work. When ePPMO-146b instead of ePNC and native exosomes, it increased the epithelial cell marker E-cadherin and suppressed the mesenchymal cell markers N-cadherin and vimentin (Fig 4G and H). These results suggested that ePPMO-146b impeded EMT by increasing E-cadherin, and decreasing N-cadherin and vimentin.

ePPMO-146b accumulates in tumors and suppresses CRC tumor growth *in vivo*

Considering that ePPMO-146b resulted in tumor suppression *in vitro* and was efficiently taken up by CRC cells, ePPMO-146b or epNC at a dosage of 5.0×10^{10} particles/kg were intraperitoneally administrated into Lovo tumor-bearing mice twice a week for 24 days (Fig 5A). Compared with the ePNC group, ePPMO-146b significantly impeded tumor growth (tumor weight inhibitory rate % = 64.71% and tumor volume inhibitory rate % = 71.12%; Fig. 5B-E). The antitumor activities of ePPMO-146b are summarized in Table 1. Of note, this exosome-mediated delivery complex did not exert systemic toxicity to tumor-bearing mice, as evidenced by stable the body weight and no deaths observed after the ePNC or ePPMO-146b treatment (Fig 5D).

Table 1

Antitumor activity of ePPMO-146b against Lovo colon cancer xenografts in nude mouse models. *n*=5, ± *s*

Drug Administration			Toxicity			Anticancer Activity			
Group	Schedule	Route	Average body weight (g, ± *s*)		Death	Tumor weight (g)	IR (%)	Tumor volume (mm^3)	IR (%)
			Start	Stop					
ePNC	BIW,4w	i.p.	16.36±0.75	17.94±0.39	0/5	0.17±0.06	-	334.31±35.28	-
ePPMO-146b	BIW,4w	i.p.	15.34±1.12	19.30±0.74*	0/5	0.06±0.02	64.71%	96.40±32.34**	71.12%

BIW=twice a week: The significance of differences (vs. epNC) was determined by one-way ANOVA with a t test. *p<0.05, **p<0.01, ***p<0.001 (n=5, ± s)

It has been demonstrated that the intraperitoneal injection of exosomes resulted in a stronger accumulation of drugs in tumors than that of intravenous injection [11]. Thus, vesicles were labeled with the lipophilic fluorescent tracer DiR. The fluorescence intensity of free-DiR, DiR-exosomes, DiR-ePNC, and DiR-ePPMO-146b was evaluated in nontumor-bearing mice. DiR-ePNC and DiR-ePPMO-146b,and DiR-exosomes were mainly distributed in the liver *in vivo* by i.p. after 3 h and *ex vivo* at 6 h postinoculation, which is consistent with a previous study on the biodistribution of exosomes[31] (Fig 5G - H), indicating that the exosome-mediated delivery complex (ePNC and ePPMO-146b) resulted in a stronger accumulation in the liver than that of the unloaded exosome group.(Fig 5H).

Additionally, an ideal anticancer drug delivery system following systemic administration should be characterized by tumor accumulation, therefore the *in vivo* biodistribution of ePPMO-146b was investigated in tumor-bearing mice. Similar to non-tumor-bearing mice, fluorescent signal was still detected in liver while some were found dramatical accumulation in tumor sites, suggesting a specific retention of exosomes in tumors (Fig 5I-K). All these data revealed that ePPMO-146b efficiently targeted PMO to the tumor sites while reserving its robuster accumulation in the liver compared to that of unloaded exosome.

Discussion

In the present study, we developed a hUC-MSC-derived exosome-based drug delivery strategy by loading CP05-PMO-146b onto the surface of exosomes. ePPMO-146b successfully induced a therapeutic effect on CRC progression by inhibiting EMT *in vitro* and *in vivo*, which was in accordance with our previous work[19]. Of particular importance, this MSC-derived exosomes system did not induce any cellular and systemic toxicity and was able to deliver the payload safely and effectively with excellent ability to target the tumors. The resulting hepatic accumulation also suggested that an inhibitory effect occurred on the live metastasis of CRC. To our knowledge, ePPMO-146b represents the first potential practice of exosomes in the application of PMO-146b-based antimetastatic therapy to overcome the translational limitation of oligonucleotides in CRC.

Because anticancer chemotherapeutic drugs cause severe side effects, a new drug pipeline needs to minimize the toxicity of a drug while ensuring that it accumulates in target tissue. For example, to date, fluoropyrimidines are still the first-line conventional chemotherapy for mCRC treatments. However, fluoropyrimidines indiscriminately destroy normal cells and cause toxic side effects, and a gradually developed multidrug resistance introduces clinical challenges to physicians[35]. Due to the lack of specific targets of chemotherapy drugs, targeted therapies, such as monoclonal antibodies and small molecule inhibitors, are sought out. In the manufacturing scale of biomedicines, the process of developing monoclonal antibodies is unsustainable and has emerged as an industrial bottleneck[36]. In addition, conventional small-molecule pharmaceuticals entail much larger, and often iterative, screening efforts, which are followed by extensive steps of optimizing medicinal chemistry parameters[1]. MiRNA-based therapy appears to be a very ingenious and promising approach for gene therapy with mCRC. Recently, some miRNA drugs have been approved to enter clinical trials on indications other than solid tumors, such as cutaneous T-cell lymphoma and Alport syndrome[37, 38]. Many data have demonstrated a definitive protumorigenic role of miR-146b in CRC, suggesting that ASO-miR-146b is feasible for developing a targeted drug[19–21]. To overcome the poor cellular uptake of oligonucleotide drugs, nanotechnology has been developed for miRNA or ASO delivery. MiRNA delivery is optimized using either viral or nonviral methods. Viral delivery of synthetic miRNA has been demonstrated to be very efficient; however, immunogenicity remains a bottleneck for clinical application. In the context of nonviral methods, exosomes, as “natural” delivery vehicles that are nontoxic and are produced in an autologous manner, are capable of transferring therapeutic molecules (such as nucleic acids and recombinant proteins) into cancer cells. The following strategies have been developed to optimize the “cargo” loading of exosomes: (1) transfect therapeutic miRNAs or miRNA expression vectors into parental cells; then, miRNAs are subsequently enclosed in exosomes endogenously. For example, lenti-miR-128-3p was transfected into normal intestinal FHC cells, and exosomes were isolated and resensitized CRC to oxaliplatin[39]. (2) Exosomes were isolated from donor cells followed by the application of artificial internalization methods (such as electroporation, sonication, and surface functionalization with lipophilicity conjugation) to exogenously introduce therapeutic miRNAs into vesicles. For example, ASO-miRNA-221 was loaded into exosomes from MSCs by electroporation to treat CRC[40]. (3) The external membrane of isolated exosomes was chemically modified. Chemical modification does not involve tedious gene engineering and the low efficiency of internalizing, thus the technique is deemed as an easily attainable alternative that is highly efficient in loading exosomes with therapeutics. Regarding the *in vivo* digestive circumstance, the ASO synthesized with PMO is an ideal resolution. PMOs are a charge-neutral class of antisense agents that interfere with target transcripts either by binding or by sterically blocking the assembly of translation machinery, resulting in enhanced oligonucleotide drug delivery[41]. Although PMOs are a new generation of antisense oligomers with a relatively high specificity and efficacy, the transportation of PMOs into cells can only be implemented via physical methods with low bioavailability rather than with transfection reagents[24]. Importantly, Gao et al. reported that the CP05 peptide (CRHSQMTVTSRL) enabled PMOs to conjugate exosomes by anchoring to CD63. In this study, we addressed the most relevant challenges in applying exosomes as vehicles to load PMO-146b for

directed colon cancer therapy (Figs. 4 and 5), and the process from cellular uptake (Fig. 3A) to biodistribution and safe systemic delivery were included (Fig. 5).

Despite the remarkable advances and successes of exosomes in the field of drug delivery, there are increasing concerns about cellular production and reliable sources of EVs[8]. MSCs are the only human cell type amenable to scalable production of exosomes and have been exploited to clinical grade[11]. Since it is vital to perform repeatable measurement of EV concentration for further application in drug delivery, critical quality attributes (CQAs), such as particle size distribution (PSD), particle concentration (quantification of particle number per unit of volume) and phenotype, are indispensable[42]. Different techniques have been applied to measure physical EV properties, and these techniques include multiangle dynamic light scattering (MADLS), asymmetric flow field flow fractionation coupled with multiangle light scattering (AF4-MALS), centrifugal liquid sedimentation (CLS), nanoparticle tracking analysis (NTA), tunable resistive pulse sensing (TRPS) and high-sensitivity nanoflow cytometry (nFCM)[42]. NTA is the most frequently used approach, but Vogel R et al. reported that NTA had to be averaged over three independent runs with CVs (CV = standard deviation/mean, 19%), while nanoFCM was performed just once[43]. Additionally, nanoFCM reached a nominal resolution below 100 nm through a combined implementation of fluorescence triggering, narrow laser beam, sensitive detectors and instrument configuration[43]. Accordingly, in this study, nanoFCM was applied to verify the order of magnitude of exosomes (Fig. 1B).

Exosomal cargoes have been found to correlate with the physiological state of donor cells. Isolated tonsil-derived MSC-secreted EVs possessed a tumor suppressive effect on the human liver cancer cell line HepG2[44]. Due to their multipotency, MSC-derived exosomes could also be tumorigenic[45]. Bone marrow MSC-derived exosomes favored tumor growth *in vitro* and *in vivo*[46]. Compared to other MSC origins, hUC-MSCs are preferred for cell-free therapies because they have the lowest tumorigenic ability, do not have ethical concerns, and utilize a noninvasive isolation procedure; in addition, hUC-MSCs exhibit a lower immunogenicity, faster self-renewal ability, more stable doubling time and higher proliferation potency[47]. Nevertheless, there is no evidence of whether hUC-MSC-derived exosomes promote CRC development. Therefore, the appropriate concentration of hUC-MSC-exosomes was ascertained in this study by CCK8 assays (Fig. 3C). hUC-MSCs are well suited for the mass production of exosomes at 10^9 particles/mL, which is ideal for drug delivery *in vitro*.

We confirmed the tumorigenic role of miR-146b in CRC, whereas the antitumor effect of hUC-MSC-derived exosome-based delivery of PMO-146b is still unknown. Based on this issue, the CP05 peptide acted as a bridge to link PMOs and exosomes to facilitate the systemic delivery of PMO-146b. Unfortunately, we could not directly quantify miR-146b by qRT–PCR because of the charge-neutral phosphoramidate linkages of PMO. The PKH67-labeled MSC-exosomes that were co-incubated with biotin-conjugated PMO-146b in SW620 cells and were detected by streptavidin-conjugated PE via flow cytometry indirectly verified that the MSC-exosomes were efficiently loaded with PMO (Fig. 2) and delivered PMO into SW620 cells (Fig. 3A). When cellular ePPMO-146b reached the definite concentration, CRC cell viability was obviously inhibited (Fig. 3D), and consistent with anti-miR-146b, ePPMO-146b resulted in an inhibitory effect on the EMT phenotypes of CRC (Fig. 4). The major advantages of the exosome delivery system include its minimal toxicity and the resulting hepatic accumulation *in vivo*. EPPMO-146b inhibited the growth of transplanted tumors to a certain extent, while the body weight of tumor-bearing mice in both the ePPMO-146b and epNC (control) groups remained within a stable baseline (Fig. 5A-F). Preliminary experiments were also performed on the systemic distribution of exosomes in nontumor and tumor-bearing mice, and exosomes were observed mainly located in the liver and tumor (Fig. 5H&J). The liver enrichment was enhanced when exosomes were loaded with PPMO-146b, indicating that ePPMO-146b was a precise delivery platform for ASO. It is worth noting that the liver is the major target organ of mCRC, so we speculate that ePPMO-146b can play important roles not only in targeted treatment of the primary tumor but also in curing the hepatic metastasis of mCRC.

Conclusion

Our findings demonstrated that hUC-MSCs are a reliable source of exosomes and that MSC-exosomes are among the best candidates for miRNA-based therapeutics. In the present study, we described a hUC-MSC-derived exosome-based delivery system that loaded anti-miR-146b, namely, ePPMO-146b, into CRC tumor tissue. ePPMO-146b significantly inhibited CRC by

inhibiting EMT *in vitro* and *in vivo* and was a safe and effective CRC treatment. Our results provide a treatment modality for miRNA-based or even oligonucleotide-based therapeutics in cancer by applying hUC-MSC-derived exosomes as vehicles.

Abbreviations

colorectal cancer :CRC, human cord umbilical mesenchymal cell :hUC-MSC; antisense oligonucleotide: ASO; epithelial-to-mesenchymal transition :EMT; metastatic CRC :mCRC; anti-miRNA oligonucleotides :AMOs; small interfering RNAs :siRNAs;mesenchymal stem cells :MSCs; hepatocellular carcinoma :HCC; bone marrow MSCs :BM-MSCs; antisense oligonucleotides :ASO; phosphorodiamidate morpholino oligonucleotide :PMO; nano flow cytometry :NanoFCM; transmission electron microscopy :TEM; negative controls :NC; human leucocyte antigen-DR :HLA-DR; tumor susceptibility gene 101 protein :TSG101; US food and Drug Administration :FDA

Declarations

Ethics approval and consent to participate

This study was reviewed and approved by the Ethics Committee of Harbin Medical University Cancer Hospital, and all the participants signed an informed consent form. The animal experimental and housing procedures were performed in accordance with the protocols of Animal Experimentation and Ethics Committee of Harbin Medical University Cancer Hospital and Peking University Shenzhen Hospital

Consent for publication

All the participants involved in our study obtained written consent for publication.

Availability of data and materials

The datasets used and/or analyzed during the current study are available from the corresponding author on reasonable request. Additional information available: additional Fig. S1 Table S1.

Competing interests

The authors declare that they have no competing interests.

Funding

This work was supported by grant from the Natural Science Foundation of China (82002567), Applied Basic Research Programs of Science and Technology Department of Guangdong Province (Grant No. 2019A1515110485), Science, Technology and Innovation Commission of Shenzhen Municipality (JCYJ20190809093205533, JCYJ20210324110200002) to S.Y.. Haiyan Foundation of Harbin Medical University Cancer Hospital (Grant No. JJZD2022-02) to X.H, (Grant No.JJZD2021-04) to Q.M..

Authors' contributions

X.H. designed the experiments. S.Y. composed the draft and analyzed the data. X.H. revised the manuscript. L.B., R.L. and S.Y. conducted the most experiments. R.L., L.B. and G.M. performed the animal models. Q.M., Z.L supervised the project and commented on the project. Y.Z, Y.M.Z, and Q.Y. assisted with the experiments. S.Y., X.H., Q.M., and S.W. have provided financial support during the whole project. All authors read and approved the final manuscript.

Acknowledgements

We thank Dr. Hong M. Moulton (Biomedical Sciences, College of Veterinary Medicine, Oregon State University, USA) for her assistance in the stable amide linker synthesis which conjugated CP05 with PMO.

References

1. Roberts TC, Langer R, Wood MJA: **Advances in oligonucleotide drug delivery**. *Nat Rev Drug Discov* 2020, **19**(10):673-694.
2. Cheng L, Hill AF: **Therapeutically harnessing extracellular vesicles**. *Nat Rev Drug Discov* 2022.
3. Thery C, Witwer KW, Aikawa E, Alcaraz MJ, Anderson JD, Andriantsitohaina R, Antoniou A, Arab T, Archer F, Atkin-Smith GK *et al*: **Minimal information for studies of extracellular vesicles 2018 (MISEV2018): a position statement of the International Society for Extracellular Vesicles and update of the MISEV2014 guidelines**. *J Extracell Vesicles* 2018, **7**(1):1535750.
4. Sohrabi B, Dayeri B, Zahedi E, Khoshbakht S, Nezamabadi Pour N, Ranjbar H, Davari Nejad A, Noureddini M, Alani B: **Mesenchymal stem cell (MSC)-derived exosomes as novel vehicles for delivery of miRNAs in cancer therapy**. *Cancer Gene Ther* 2022.
5. Coelho JF, Ferreira PC, Alves P, Cordeiro R, Fonseca AC, Gois JR, Gil MH: **Drug delivery systems: Advanced technologies potentially applicable in personalized treatments**. *EPMA J* 2010, **1**(1):164-209.
6. Mulcahy LA, Pink RC, Carter DR: **Routes and mechanisms of extracellular vesicle uptake**. *J Extracell Vesicles* 2014, **3**.
7. Fujita Y, Kadota T, Araya J, Ochiya T, Kuwano K: **Clinical Application of Mesenchymal Stem Cell-Derived Extracellular Vesicle-Based Therapeutics for Inflammatory Lung Diseases**. *J Clin Med* 2018, **7**(10).
8. Yeo RW, Lai RC, Zhang B, Tan SS, Yin Y, Teh BJ, Lim SK: **Mesenchymal stem cell: an efficient mass producer of exosomes for drug delivery**. *Adv Drug Deliv Rev* 2013, **65**(3):336-341.
9. Lou G, Chen L, Xia C, Wang W, Qi J, Li A, Zhao L, Chen Z, Zheng M, Liu Y: **MiR-199a-modified exosomes from adipose tissue-derived mesenchymal stem cells improve hepatocellular carcinoma chemosensitivity through mTOR pathway**. *J Exp Clin Cancer Res* 2020, **39**(1):4.
10. Li H, Yang C, Shi Y, Zhao L: **Exosomes derived from siRNA against GRP78 modified bone-marrow-derived mesenchymal stem cells suppress Sorafenib resistance in hepatocellular carcinoma**. *J Nanobiotechnology* 2018, **16**(1):103.
11. Mendt M, Kamerkar S, Sugimoto H, McAndrews KM, Wu CC, Gagea M, Yang S, Blanko EVR, Peng Q, Ma X *et al*: **Generation and testing of clinical-grade exosomes for pancreatic cancer**. *JCI Insight* 2018, **3**(8).
12. Tang M, Chen Y, Li B, Sugimoto H, Yang S, Yang C, LeBleu VS, McAndrews KM, Kalluri R: **Therapeutic targeting of STAT3 with small interference RNAs and antisense oligonucleotides embedded exosomes in liver fibrosis**. *FASEB J* 2021, **35**(5):e21557.
13. Siegel RL, Miller KD, Fuchs HE, Jemal A: **Cancer statistics, 2022**. *CA Cancer J Clin* 2022, **72**(1):7-33.
14. Biller LH, Schrag D: **Diagnosis and Treatment of Metastatic Colorectal Cancer: A Review**. *JAMA* 2021, **325**(7):669-685.
15. Balacescu O, Sur D, Cainap C, Visan S, Cruceriu D, Manzat-Saplacan R, Muresan MS, Balacescu L, Lisencu C, Irimie A: **The Impact of miRNA in Colorectal Cancer Progression and Its Liver Metastases**. *Int J Mol Sci* 2018, **19**(12).
16. Karimzadeh MR, Zarin M, Ehtesham N, Khosravi S, Soosanabadi M, Mosallaei M, Pourdavoud P: **MicroRNA binding site polymorphism in inflammatory genes associated with colorectal cancer: literature review and bioinformatics analysis**. *Cancer Gene Ther* 2020, **27**(10-11):739-753.
17. Sun X, Lin F, Sun W, Zhu W, Fang D, Luo L, Li S, Zhang W, Jiang L: **Exosome-transmitted miRNA-335-5p promotes colorectal cancer invasion and metastasis by facilitating EMT via targeting RASA1**. *Mol Ther Nucleic Acids* 2021, **24**:164-174.
18. Brabletz S, Schuhwerk H, Brabletz T, Stemmler MP: **Dynamic EMT: a multi-tool for tumor progression**. *EMBO J* 2021, **40**(18):e108647.
19. Yu S, Li L, Tian W, Nie D, Mu W, Qiu F, Liu Y, Liu X, Wang X, Du Z *et al*: **PEP06 polypeptide 30 exerts antitumour effect in colorectal carcinoma via inhibiting epithelial-mesenchymal transition**. *Br J Pharmacol* 2018, **175**(15):3111-3130.
20. Zhu Y, Wu G, Yan W, Zhan H, Sun P: **miR-146b-5p regulates cell growth, invasion, and metabolism by targeting PDHB in colorectal cancer**. *Am J Cancer Res* 2017, **7**(5):1136-1150.
21. Shi L, Su Y, Zheng Z, Qi J, Wang W, Wang C: **miR-146b-5p promotes colorectal cancer progression by targeting TRAF6**. *Exp Ther Med* 2022, **23**(3):231.

22. Weiler J, Hunziker J, Hall J: **Anti-miRNA oligonucleotides (AMOs): ammunition to target miRNAs implicated in human disease?** *Gene Ther* 2006, **13**(6):496-502.
23. Romano G, Acunzo M, Nana-Sinkam P: **microRNAs as Novel Therapeutics in Cancer**. *Cancers (Basel)* 2021, **13**(7).
24. Ghosh C, Iversen PL: **Intracellular delivery strategies for antisense phosphorodiamidate morpholino oligomers**. *Antisense Nucleic Acid Drug Dev* 2000, **10**(4):263-274.
25. Gao X, Ran N, Dong X, Zuo B, Yang R, Zhou Q, Moulton HM, Seow Y, Yin H: **Anchor peptide captures, targets, and loads exosomes of diverse origins for diagnostics and therapy**. *Sci Transl Med* 2018, **10**(444).
26. Guo Y, Wan Z, Zhao P, Wei M, Liu Y, Bu T, Sun W, Li Z, Yuan L: **Ultrasound triggered topical delivery of Bmp7 mRNA for white fat browning induction via engineered smart exosomes**. *J Nanobiotechnology* 2021, **19**(1):402.
27. Zou Y, Li L, Li Y, Chen S, Xie X, Jin X, Wang X, Ma C, Fan G, Wang W: **Restoring Cardiac Functions after Myocardial Infarction-Ischemia/Reperfusion via an Exosome Anchoring Conductive Hydrogel**. *ACS Appl Mater Interfaces* 2021, **13**(48):56892-56908.
28. Lu LL, Liu YJ, Yang SG, Zhao QJ, Wang X, Gong W, Han ZB, Xu ZS, Lu YX, Liu D *et al*: **Isolation and characterization of human umbilical cord mesenchymal stem cells with hematopoiesis-supportive function and other potentials**. *Haematologica* 2006, **91**(8):1017-1026.
29. Abes S, Moulton HM, Clair P, Prevot P, Youngblood DS, Wu RP, Iversen PL, Lebleu B: **Vectorization of morpholino oligomers by the (R-Ahx-R)4 peptide allows efficient splicing correction in the absence of endosomolytic agents**. *J Control Release* 2006, **116**(3):304-313.
30. Theodoraki MN, Hong CS, Donnenberg VS, Donnenberg AD, Whiteside TL: **Evaluation of Exosome Proteins by on-Bead Flow Cytometry**. *Cytometry A* 2021, **99**(4):372-381.
31. Wiklander OP, Nordin JZ, O'Loughlin A, Gustafsson Y, Corso G, Mager I, Vader P, Lee Y, Sork H, Seow Y *et al*: **Extracellular vesicle in vivo biodistribution is determined by cell source, route of administration and targeting**. *J Extracell Vesicles* 2015, **4**:26316.
32. Ullah I, Subbarao RB, Rho GJ: **Human mesenchymal stem cells - current trends and future prospective**. *Biosci Rep* 2015, **35**(2).
33. Shi S, Zhang Q, Xia Y, You B, Shan Y, Bao L, Li L, You Y, Gu Z: **Mesenchymal stem cell-derived exosomes facilitate nasopharyngeal carcinoma progression**. *Am J Cancer Res* 2016, **6**(2):459-472.
34. Vakhshiteh F, Atyabi F, Ostad SN: **Mesenchymal stem cell exosomes: a two-edged sword in cancer therapy**. *Int J Nanomedicine* 2019, **14**:2847-2859.
35. Perez-Herrero E, Fernandez-Medarde A: **Advanced targeted therapies in cancer: Drug nanocarriers, the future of chemotherapy**. *Eur J Pharm Biopharm* 2015, **93**:52-79.
36. Somasundaram B, Pleitt K, Shave E, Baker K, Lua LHL: **Progression of continuous downstream processing of monoclonal antibodies: Current trends and challenges**. *Biotechnol Bioeng* 2018, **115**(12):2893-2907.
37. Kohnken R, McNeil B, Wen J, McConnell K, Grinshpun L, Keiter A, Chen L, William B, Porcu P, Mishra A: **Preclinical Targeting of MicroRNA-214 in Cutaneous T-Cell Lymphoma**. *J Invest Dermatol* 2019, **139**(9):1966-1974 e1963.
38. Zhou LY, Qin Z, Zhu YH, He ZY, Xu T: **Current RNA-based Therapeutics in Clinical Trials**. *Curr Gene Ther* 2019, **19**(3):172-196.
39. Liu T, Zhang X, Du L, Wang Y, Liu X, Tian H, Wang L, Li P, Zhao Y, Duan W *et al*: **Exosome-transmitted miR-128-3p increase chemosensitivity of oxaliplatin-resistant colorectal cancer**. *Mol Cancer* 2019, **18**(1):43.
40. Han S, Li G, Jia M, Zhao Y, He C, Huang M, Jiang L, Wu M, Yang J, Ji X *et al*: **Delivery of Anti-miRNA-221 for Colorectal Carcinoma Therapy Using Modified Cord Blood Mesenchymal Stem Cells-Derived Exosomes**. *Front Mol Biosci* 2021, **8**:743013.
41. Amantana A, Iversen PL: **Pharmacokinetics and biodistribution of phosphorodiamidate morpholino antisense oligomers**. *Curr Opin Pharmacol* 2005, **5**(5):550-555.

42. Vogel R, Savage J, Muzard J, Camera GD, Vella G, Law A, Marchioni M, Mehn D, Geiss O, Peacock B *et al*: **Measuring particle concentration of multimodal synthetic reference materials and extracellular vesicles with orthogonal techniques: Who is up to the challenge?** *J Extracell Vesicles* 2021, **10**(3):e12052.
43. Choi D, Montermini L, Jeong H, Sharma S, Meehan B, Rak J: **Mapping Subpopulations of Cancer Cell-Derived Extracellular Vesicles and Particles by Nano-Flow Cytometry**. *ACS Nano* 2019, **13**(9):10499-10511.
44. Choi DW, Cho KA, Kim J, Lee HJ, Kim YH, Park JW, Woo SY: **Extracellular vesicles from tonsilderived mesenchymal stromal cells show antitumor effect via miR199a3p**. *Int J Mol Med* 2021, **48**(6).
45. Phan J, Kumar P, Hao D, Gao K, Farmer D, Wang A: **Engineering mesenchymal stem cells to improve their exosome efficacy and yield for cell-free therapy**. *J Extracell Vesicles* 2018, **7**(1):1522236.
46. Zhu W, Huang L, Li Y, Zhang X, Gu J, Yan Y, Xu X, Wang M, Qian H, Xu W: **Exosomes derived from human bone marrow mesenchymal stem cells promote tumor growth in vivo**. *Cancer Lett* 2012, **315**(1):28-37.
47. Yaghoubi Y, Movassaghpour A, Zamani M, Talebi M, Mehdizadeh A, Yousefi M: **Human umbilical cord mesenchymal stem cells derived-exosomes in diseases treatment**. *Life Sci* 2019, **233**:116733.

Figures

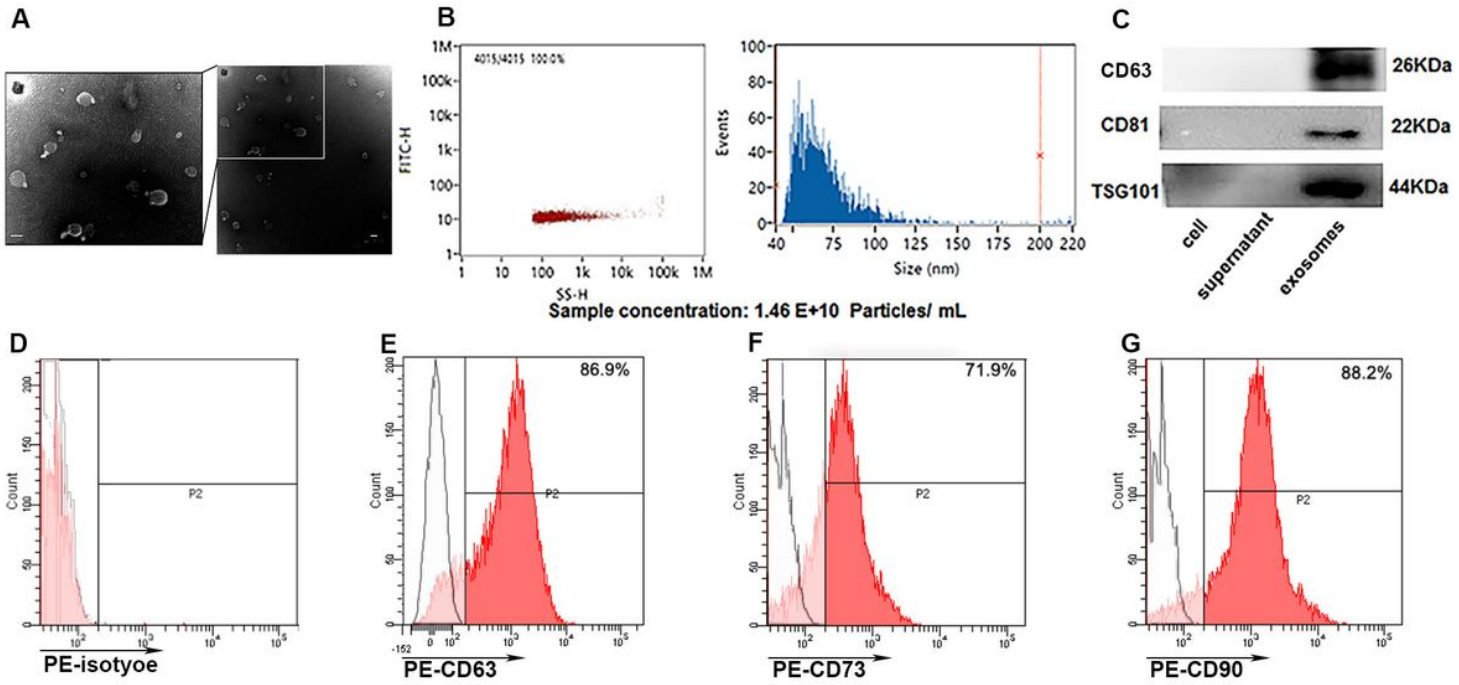

Figure 1

Characterization and identification of MSC-derived exosomes.

(A) The morphology of MSC-derived exosomes was identified under a transmission electron microscope to have a diameter of approximately 100 nm. Scale bar: 100 nm.

(B) Particle concentration of extracellular vesicles from MSCs detected by NanoFCM (left panel). The size distribution of MSC-derived exosomes was measured by NanoFCM. Mean value: 69.04 nm (right panel).

(C) The expression of specific surface markers of exosomes (CD63, CD81 and TSG101) was detected by Western blot in MSC cell lysate, culture medium postexosome isolation, and MSC-derived exosomes. Surface expression of exosome-enriched tetraspanin CD63 (E) and MSC surface markers CD73 (F) and CD90 (G) on exosome membranes was analyzed by FCM. The PE-isotype was used as a negative control (D).

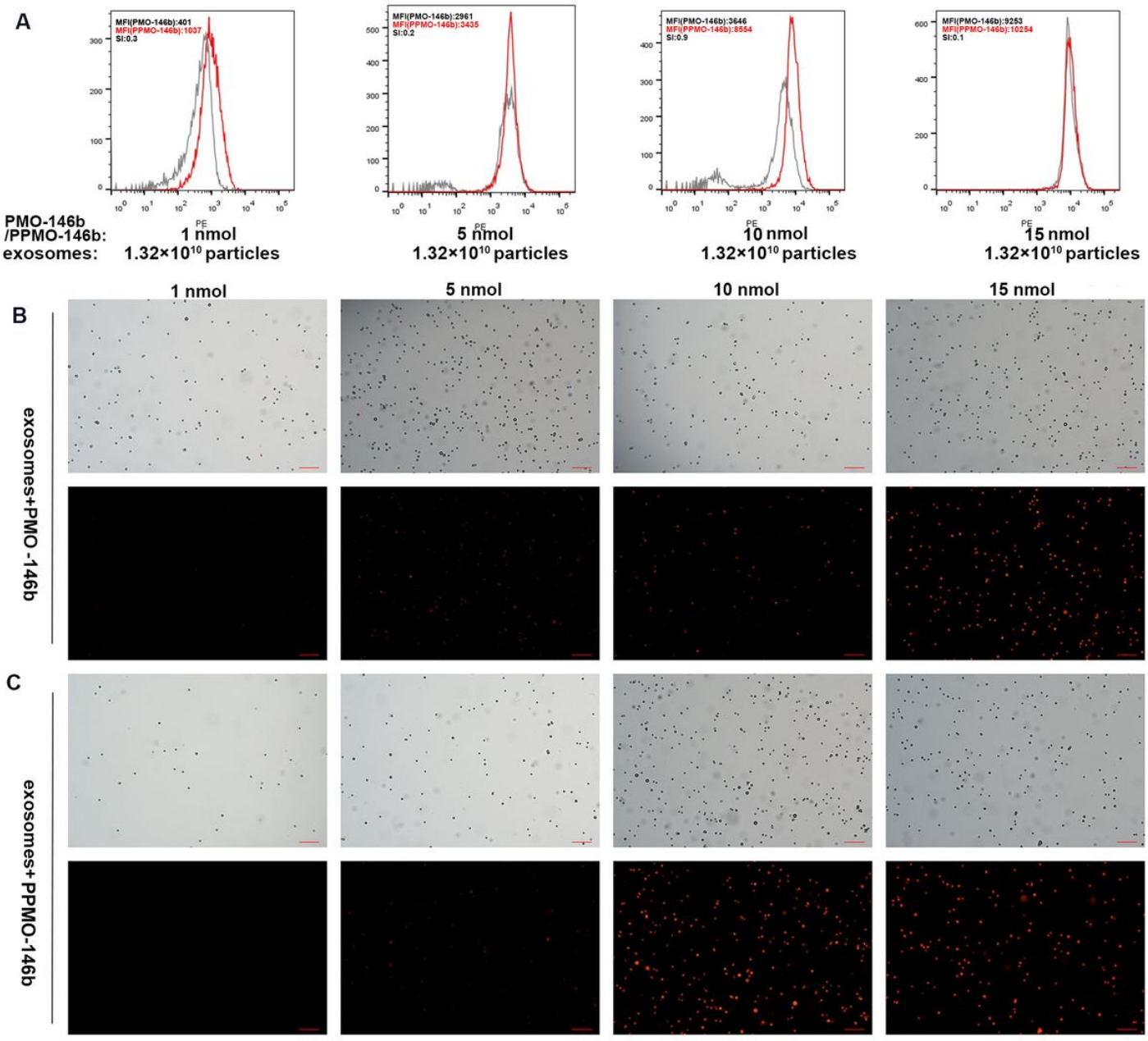

Figure 2

Establishment of the exosome/PMO-146b (PMO and PPMO) ratio via detection with streptavidin-PE. Aldehyde/sulfate latex beads were precoated with exosomes at a concentration of 1.32×10^{10} particles, followed by coincubation with increasing moles of biotinylated PMO-146b with or without CP05 peptide (PMO/PPMO).

(A) Detection was performed with pretitered streptevidin-PE. Capture was performed with biotin-labeled PMO or PPMO peptide. The ratio of 10 nmol PMO/PPMO/1.32×10^{10} exosomes produced the optimal SI at 0.9. The SI value of calculation is based on the difference in MFI between PMOs and PPMOs that were incubated with MSC-derived exosomes and the average spread of their distributions.

Different concentrations of exosome-PMO-146b (B) and exosome-PPMO-146b (C) complexes were prepared using the same procedure above and were viewed under conventional fluorescence microscopy after the beads were recovered. Upper: bright field, Under: fluorescence. Scale bar: 200 μm.

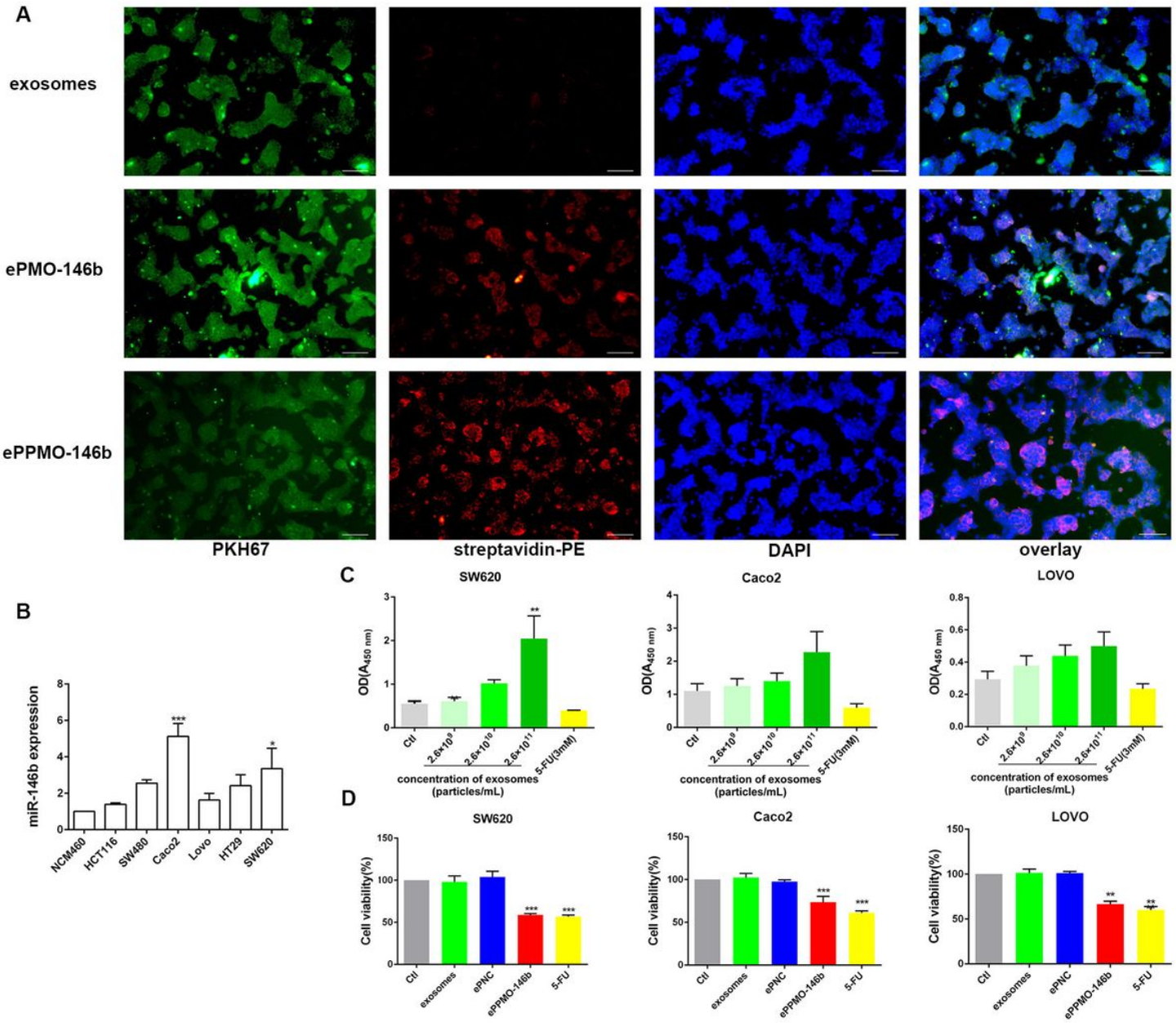

Figure 3

ePPMO-146b could be internalized by recipient cells and inhibited CRC cell viability.

(A) MSC derived exosomes labeled with PKH67 were co-incubated with biotin-labeled PMO-146b with or without CP05 and were subsequently added to SW620 cells, followed by incubation with streptavidin-PE and visualization under fluorescence microscopy. Note the intracellular localization of the labeled exosomes. The control involved the uptake of exosomes by SW620 cells in the absence of PMO-146b. Scale bar: 100 μm.

(B) qRT–PCR illustrated that the expression of miR-146b was upregulated in six CRC cell lines compared with NCM460 cells.

(C) The viabilities of the SW620, Caco2 and Lovo cells exposed to native exosomes were determined by a CCK8 assay to determine the optimal concentration. Averaged data (mean ± SEM, n = 3) of OD at 570 nm. **p<0.01 by one-way ANOVA.

(D) The relative cell proliferation ratio was normalized to the cell index of the SW620, Caco2, and Lovo cells treated with solvent (PBS, Ctl, same as below) after 48 h. MSC-exos-loaded PMO-146b (ePPMO-146b) inhibited cell growth, as

demonstrated by the CCK-8 assay. Averaged data (mean ± SEM, n = 3) of OD at 570 nm. *p<0.05, **p<0.01, ***p<0.001 by one-way ANOVA.

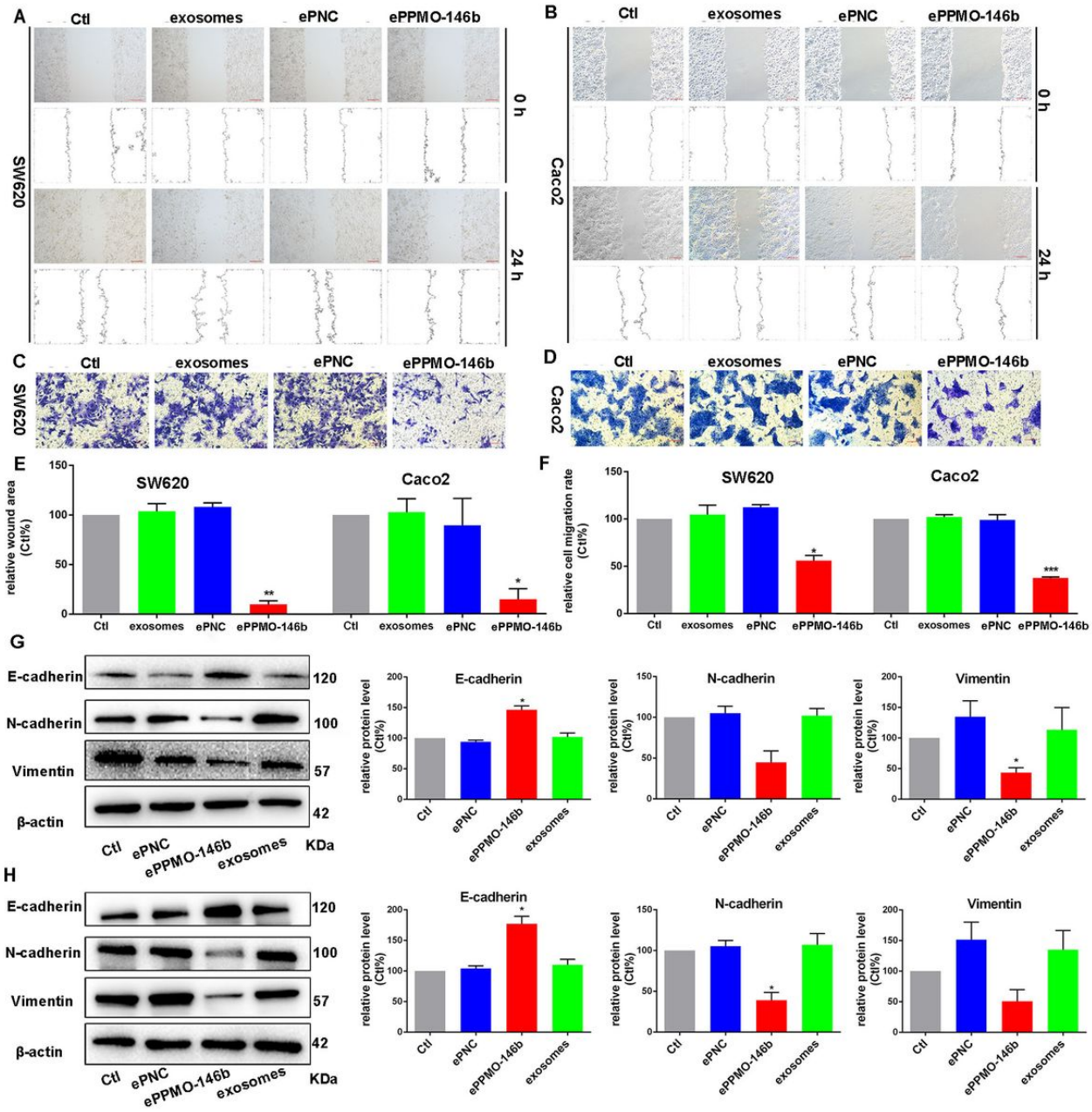

Figure 4

Inhibitory effect of ePPMO-146b on EMT in SW620 and Caco2 cells.

SW620 cells (A) and Caco2 cells (B) were treated with native exosomes, ePNC and ePPMO-146b for 24 h. ePPMO-146b significantly inhibited the migration of SW620 cells (A) and CaCO2 cells (B), as demonstrated in a wound healing assay. Scale bar: 200 μm. ePPMO-146b successfully reduced the ability of SW620 cells (C) and Caco2 cells (D) to migrate, while the native exosomes exerted no obvious effect on metastasis, as indicated by the transwell assay. Scale bar: 100 μm. (E) Column charts were plotted based on the averaged data (mean±SEM, n=3) from the wound healing assay, which shows the effective suppression effect of ePPMO-146b on migration. *P <0.05, **P < 0.01 by one-way ANOVA, Dunnett's test: compared with Ctl. (F) Column charts were plotted based on the averaged data (mean±SEM, n=3) from the transwell migration assay, which shows the effective suppression effect of ePPMO-146b on migration. *P <0.05, ***P < 0.001 by one-way ANOVA, Dunnett's test: compared with Ctl. The effects of ePPMO-146b on the expression of EMT markers in SW620 (G) and Caco2 cells (H) were

observed by Western blot analysis. β-actin was used as a sample loading control. ePPMO-146b increased E-cadherin but decreased N-cadherin and vimentin compared with Ctl. Averaged data (mean ± SEM) from three independent experiments. * P < 0.05 by one-way ANOVA, Dunnett's test: compared with Ctl.

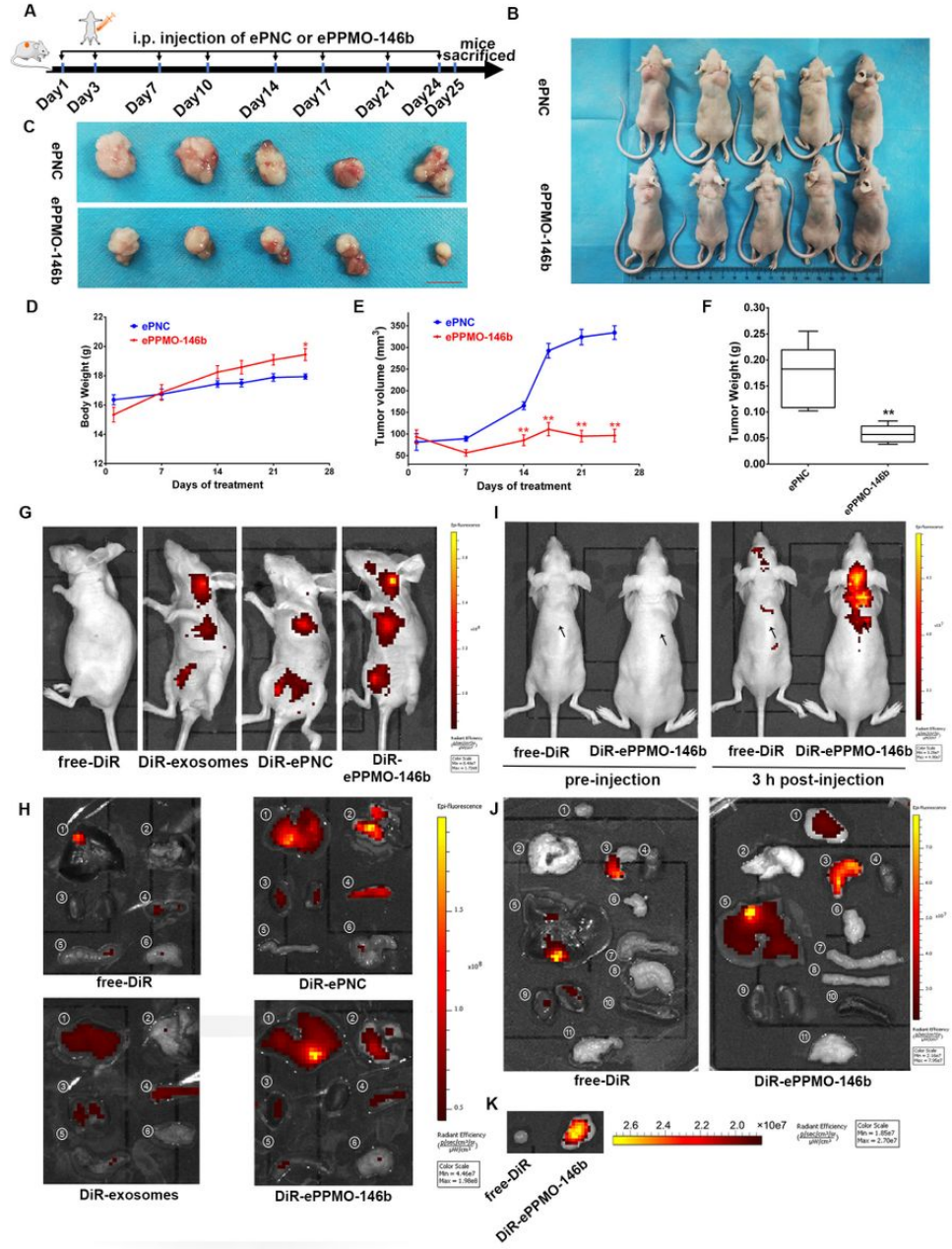

Figure 5

In vivo antitumor effect and the biodistribution of ePPMO-146b in mice.

(A) Schematic representation of the treatment (ePNC or ePPMO-146b) in Lovo tumor-bearing nude mice via i.p. administration.

(B) Representative photograph of Lovo xenograft nude mice treated with ePNC or ePPMO-146b at the end point. Exosome doses: 5.0×10^{10} particles/kg.

(C) Photograph of the tumors dissected from xenograft mice after the last treatment. Scale bar: 1 cm.

(D-F) Body weight and tumor growth during the follow-up are shown. The mouse weight was unaffected by PMO-146b-loaded exosomes. The tumor growth curve indicated the suppression of tumor growth by ePPMO-146b. *P <0.05 and **P <0.01 by

one-way ANOVA, Dunnett's test: compared with ePNC.

(G) Representative IVIS images of the live mice injected with free-DiR-treated control, untargeted DiR-exosomes, DiR-ePNC, and DiR-ePPMO-146b via i.p. at 3 h postinjection.

(H) Representative IVIS images of the different organs harvested at 6 h following the i.p. infusion of DiR-labeled ePNC or ePPMO-146b in nontumor-bearing nude mice (1-liver, 2-heart and lung, 3-kidney, 4-spleen, 5-intestine, 6-reproductive organ). The control groups received DiR dye alone (free-DiR) to determine the background.

(I) Fluorescent images of LoVo tumor-bearing mice 3 h postinjection of free DiR or DiR-ePPMO-146b. The arrow indicates where the tumor was located.

(J) Fluorescent images of the major organs (6 h post-injection) harvested from mice (1-tumor, 2-lung, 3-stomach, 4-heart, 5-liver, 6-pancreas, 7-intestine, 8-colon, 9-kidney, 10-spleen, 11-reproductive organ).

(K) Representative IVIS images of the tumors at 3 h postinjection of DiR-labeled ePPMO-146b.

Supplementary Files

This is a list of supplementary files associated with this preprint. Click to download.

- FigureS1.tif
- tableS1.docx
- graphicabstract.jpg